J. Fluid Mech. (1989), *vol.* 209, *pp.* 227–247
Printed in Great Britain

The role of the surface density field in subtropical gyre circulation

By G. S. JANOWITZ

Department of Marine, Earth and Atmospheric Sciences, North Carolina State University, Raleigh, NC 27695-8208, USA

(Received 20 February 1988 and in revised form 5 May 1989)

The effects of the surface density field on wind-driven subtropical gyre circulation are examined within the content of a continuously stratified, potential vorticity conserving model. It is found that the ventilated fluid downwelled from the mixed layer is confined to a relatively thin layer in subtropical regions; the maximum depths of the ventilated region occur in the eastern and southern regions of the gyre. As a consequence of the relative thinness of the ventilated region in the wind-driven gyre, the transport associated with the surface density field is a small part of the total transport in subtropical regions. Thus the surface density field and the potential vorticity associated with ventilated fluid play a minor role in subtropical gyre dynamics and the potential vorticity of unventilated recirculating fluid is found to play the major role in subtropical gyre dynamics. A method of calculating the flow in the relatively large recirculating region is developed and the results of a specific example are discussed.

1. Introduction

In the past decade, there has been a renewal of interest in the baroclinic aspects of wind-driven subtropical gyre circulation. While a theory of the vertically averaged wind-driven basin-scale circulation has been accepted for decades, newly available data and theoretical approaches have increased our insight into the vertical structure of the wind-driven mid-latitude gyre; see Rhines (1986) for a review of recent progress in this area.

Baroclinic effects are due both to the overall vertical variation in potential density, $\Delta\rho v$, from a mean ρ_0 as well as to surface density variations of scale $\Delta\rho h$ ($\lesssim \Delta\rho v$). If D is the depth of the wind-driven gyre, Ω and r the rotation rate and radius of the earth, and W the magnitude of the wind-driven surface Ekman suction velocity, then the wind-driven tilt of the isopycnal surfaces give rise to a transport of order $g\Delta\rho v D^2/2\Omega r\rho_0$. Setting this equal to the wind-driven transport ($o(Wr)$) yields an estimate for D of $O(2\Omega Wr^2/g\Delta\rho v/\rho_0)^{\frac{1}{2}}$, approximately 1 km. Now if the imposed surface density field has a depth of influence H, then the transport associated with the surface density field is of order $(H/D)^2$ relative to the total transport. In the present non-diffusive work, we take H to be the depth to which parcels leaving the surface sink. Although on dimensional grounds H is of order D the ratio H/D may be numerically small. As the depth of influence H is determined by the flow itself, we cannot make an *a priori* estimate of the importance of the surface density field on the overall dynamics. Our principal objective in this work is to determine the spatially

varying ratio, H/D, and so determine the relative importance of the surface density field on gyre dynamics.

The principal theoretical models that have been used to study baroclinic aspects of subtropical gyre circulation are layered models in which the potential vorticity is conserved in layers or portions of layers not exposed to direct wind forcing. These models are developed in the works of Rhines & Young (1981), Pedlosky (1983) and Luyten, Pedlosky & Stommel (1983). Unventilated models, in which the uppermost layer extends to the gyre's lateral boundaries exclude the effect of the surface density field while ventilated models force H/D to be order one by their formulation. Thus layered models, as thusfar developed, cannot be used to explore the relative significance of the surface density field.

Recently, the author (Janowitz 1986; hereinafter referred to as J), developed a continuously stratified potential-vorticity-conserving model utilizing the potential density and vertical coordinates as independent and dependent variables respectively. In J, following a general formulation, the implications of a postulated form of the potential vorticity were explored. The results for that form of the potential vorticity function showed that some isopycnal surfaces were totally unventilated, some were partially and others were totally ventilated. As far as the form of the potential vorticity function, no effort was made to distinguish between parcels of surface origin, ventilated parcels, and parcels of sidewall origin, unventilated or recirculating parcels, despite their very different previous histories in dissipative layers.

In this paper, to study the effect of the surface density field on gyre structure, we shall partition the potential vorticity function as to the point of entry of a parcel into the gyre. The potential vorticity of unventilated recirculating parcels of sidewall origin will be taken to be a function of density alone; this specification is consistent with the observations presented in Rhines (1986). The potential vorticity function of ventilated parcels downwelling from the free surface will initially be left completely general. This explicit partitioning of the potential vorticity function is essential to explore surface density effects. Following our numerical calculations, we shall compare model predictions with the results of Cox & Bryan (1984), Pedlosky & Young (1983), Kilworth (1987) and Huang (1986). Before turning to a partitioned model we briefly review the general development as given in J.

2. Model development

We consider a steady, inviscid, continuously stratified flow in geostrophic balance. The flow region is bounded from above by the base of the mixed-layer region, here taken as $z = 0$, where the surface density and the negative vertical Ekman suction velocity, $w_E(\lambda, \theta)$ is specified. The flow region is bounded from below, at $z = -H_b(\lambda, \theta)$, the thermocline base, by a stagnant region of uniform potential density, ρ_1. The lateral boundaries are the northern and southern latitudes θ_n and θ_s at which $w_E = 0$ and rigid vertical walls at the longitudes $\lambda = 0$ and λ_e. At the eastern wall, λ_e, the zonal transport is taken to vanish. In what follows, the subscripts 0, b, e, w, n, s and p denote variables evaluated at the surface, thermocline base, eastern wall, western wall, θ_n, θ_s and the partitioning surface (discussed later) respectively. We take W to be the maximum value of $|w_E|$, r the Earth's radius, D a vertical scale, $\Delta\rho/\rho_1$ a scale for potential density variations. The density equation of state is taken to be $\rho = p/C_s^2 + \rho_\theta$, where C_s is a constant speed of sound and ρ_θ is the conservative

potential density field. With overbars denoting dimensionless parameters, we non-dimensionalize as follows.

$$\left.\begin{aligned} z = D\bar{z}, \quad \omega_E &= W\bar{w}_0, \\ (u, v) &= (Wr/D)(\bar{u}, \bar{v}), \\ \rho_\theta = \rho_1 - \Delta\rho\bar{t}, \quad p &= p_1(z) + \Delta\rho g D\bar{p}, \\ \frac{dp_1}{dz} &= -g\rho_1 - gp_1/C_s^2, \\ \bar{P} &= \bar{p} - z\bar{t}, \\ \frac{\Delta\rho}{\rho_1} D^2 &= 2\Omega W r^2/g = \alpha. \end{aligned}\right\} \tag{1}$$

We note that $\Delta\rho/\rho_1$ and D cannot be specified independently as α is specified. The variable-t replaces ρ used in J. Requiring that $W/2\Omega D$, gD/C_s^2 be small compared to one, dropping the overbars on dimensionless variables, and utilizing the Bernoulli function, P, the governing equations in (λ, θ, t) coordinates, as derived in J, are as follows.

$$\sin\theta \boldsymbol{\kappa} \times \boldsymbol{v} = -\nabla P, \tag{2a}$$

$$P_t = -z, \tag{2b}$$

$$(uz_t)_\lambda + (v\cos\theta z_t)_\theta = 0, \tag{2c}$$

$$w = uz_\lambda/\cos\theta + vz_\theta, \tag{2d}$$

$$\nabla = \boldsymbol{e}_\lambda(\,)_\lambda/\cos\theta + \boldsymbol{e}_\theta(\,)_\theta. \tag{2e}$$

We note that the derivatives with respect to λ and θ are taken at constant t. When $(2a)$ is used in $(2c)$, the continuity equation, the following potential vorticity equation results.

$$P_{tt} = -\sin\theta\pi(P, t). \tag{3a}$$

The potential vorticity function in (3) is the inverse of the conventional potential vorticity, i.e. $\pi = (-\sin\theta\rho_z)^{-1}$. The boundary conditions on $(3a)$ are as follows:

at $t = t_0$,
$$z = -P_t(\lambda, \theta, t_0) = 0, \tag{3b}$$

$$w(\lambda, \theta, t_0) = w_0(\lambda, \theta); \tag{3c}$$

at $t = 0$,
$$P(\lambda, \theta, 0) = 0; \tag{3d}$$

at $\lambda = \lambda_e$,
$$\int_{-H_b}^{0} u\,dz = \int_0^{t_0} uz_t\,dt = 0. \tag{3e}$$

In J, conditions $(3c)$ and $(3e)$ can be combined into a single 'Sverdrup' condition.

$$\int_0^{t_0} P_t^2\,dt = -2\sin^2\theta \int_\lambda^{\lambda_e} w_0(\lambda', \theta)\,d\lambda' + C \equiv S(\lambda, \theta). \tag{4}$$

We note that
$$\boldsymbol{M} = \int_{-H_b}^{0} \boldsymbol{v}\,dz = \boldsymbol{\kappa} \times \nabla S/\sin\theta$$

is the vertically integrated transport. If the constant C is chosen to be the zero, the thermocline base surfaces at λ_e and other points where the integral vanishes. This

leads to singular velocities at these points. As in J, we eschew this choice for C and take $C > 0$. Also we take $\lambda_e = 1.1$, $\theta_s = 12°$, $\theta_n = 52°$, and

$$w_0 = -\sin(4.5(\theta - \theta_s)). \tag{5}$$

Thus w_e vanishes at θ_s, θ_n and is negative for $\theta_s < \theta < \theta_n$. For this choice of w_0

$$S(\lambda, \theta) = 2\sin^2\theta \sin(4.5(\theta - \theta_s))(\lambda_e - \lambda) + C. \tag{6}$$

A solution useful in this present paper is obtained by setting $\pi = 1.0$ in $(3a)$ and integrating that equation subject to $(3b)$, $(3d)$ and (4). We find

$$P = \sin\theta(t_0 t - \tfrac{1}{2}t^2), \tag{7a}$$

$$t_0 = (3S/\sin^2\theta)^{\frac{1}{3}}, \tag{7b}$$

$$H_b = (3S\sin\theta)^{\frac{1}{3}}, \tag{7c}$$

$$P_0 = P(\lambda, \theta, t_0) = \tfrac{1}{2}\sin\theta t_0^2 = \tfrac{1}{2}(9S^2/\sin\theta)^{\frac{1}{3}}, \tag{7d}$$

$$H_b(\lambda_e, \theta) = (3C\sin\theta)^{\frac{1}{3}}, \tag{7e}$$

$$t_0(\lambda_e, \theta) = (3C/\sin^2\theta)^{\frac{1}{3}}, \tag{7f}$$

$$u(\lambda_e, \theta, t) = -\cos\theta(\tfrac{1}{3}t_0 t - \tfrac{1}{2}t^2)/\sin\theta, \tag{7g}$$

$$u(\lambda_e, \theta, \tfrac{1}{3}t_0) = -\cos\theta t_0^2/18\sin\theta. \tag{7h}$$

Although the solution given in (7) will be discussed in detail later, a few points should be discussed now. For a value of $C = 0.15$ we find that at $\lambda = 0$, $u_0 \geqslant 0$ for $37° = \theta_w^* \leqslant \theta \leqslant \theta_n = 52°$. Further, nearly all the fluid at $\lambda = 0$, $37° \leqslant \theta \leqslant 52°$, is outflowing from the western boundary ($u > 0$) or if inflowing, the values of P indicate that the limited region of inflowing parcels originated further to the north at $\lambda = 0$ and flowed clockwise back into the western boundary. Hence all parcels at $\lambda = 0$, $37° \leqslant \theta \leqslant 52°$ are of western boundary, as opposed to surface, origin. This point will be taken up again later. The results given in $(7e)$–$(7h)$ hold at the eastern boundary ($\lambda = \lambda_e$). The thermocline depth increases monotonically to the north. The zonal speed is negative for $0 \leqslant t \leqslant \frac{1}{3}2t_0$ or $-H_b \leqslant z \leqslant -\frac{1}{3}H_b$ and positive above this depth. The outflow is most negative at $t = \frac{1}{3}t_0$ ($z = -\frac{1}{3}2H_b$) with its magnitude given in $(7h)$. The total efflux from the eastern boundary below $-\frac{1}{3}H_b$, which is balanced by the influx above this depth is given by

$$Q = \int_{\theta_s}^{\theta_n} d\theta \int_{-H_b}^{-\frac{1}{3}H_b} u\, dz = 0.26C,$$

and the mean outflow speed (Q divided by the entire area of outflow) is $0.53C^{\frac{2}{3}}$. We shall use these results in §6. The choice of $\pi = 1$ implies that the dimensional conventional vorticity $\pi_c^* = 2\Omega\Delta\rho/\rho_1 D$. With the parameter α in equation (a) specified, if $\Delta\rho/\rho_1$ is specified, D and π_c^* follow. If π_c^* and α are specified, $\Delta\rho/\rho_1$ and D follow. Reasonable values for α and π_c^* lead to $\Delta\rho/\rho_1 = O(10^{-3})$ and $D = O(1\text{ km})$ which are also reasonable.

We now turn to the problem of specifying a partitioned model, one in which the point of origin of a parcel determines the nature of the potential vorticity function.

3. Specification of a partitioned model

At the northern boundary we take t_{0n} to be independent of λ. As $w_0 = 0$ there, $v \equiv 0$ at $\theta = \theta_n$. South of this boundary we require that $t_0 > t_{0n}$ so that isopycnal surfaces with t less than t_{0n} do not outcrop and are unventilated; a deep unventilated region must therefore exist. Near the surface, fluid has just emerged from the mixed layer and is ventilated so that near the surface a ventilated region must exist. We now postulate that one deep ventilated and one shallower unventilated region exist for all λ, θ; the two-layer assumption is the most reasonable and simplest one we can make and conditions for the consistency of this model will be discussed.

For $-H_b(\lambda, \theta) \leqslant z \leqslant -H_p(\lambda, \theta)$, the fluid is unventilated and for $-H_p < z \leqslant 0$, the fluid is ventilated. At the partitioning depth $H_p(\lambda, \theta)$, the density is $t_p(\lambda, \theta)$; both H_p and t_p must be determined. At the northern boundary $H_p = 0$ and $t_p = t_{0n}$. The fluid in both regions is assumed to be in motion as there is not observational evidence to the contrary.

The potential vorticity in the unventilated region is taken to be homogenized, i.e. for $0 \leqslant t \leqslant t_p$, $\pi = f(t)$ (> 0). Normally $\mathrm{d}f/\mathrm{d}t \leqslant 0$ so that the magnitude of ρ_z increases as we move upwards from the thermocline base through the unventilated region, although this is not required by the model. The potential vorticity in the unventilated region is totally general and is taken to be consistent to the surface density field and the underlying dynamics. Both P and P_t must be continuous as t increases through $t_p(\lambda, \theta)$; this condition ensures continuity of the velocity field across the partitioning surface. Isopycnal surfaces which outcrop will be above the partitioning surface in some regions, see figure 1.

With $f(t)$ specified we can integrate equation $(3a)$ subject to $(3d)$ to obtain the following for $0 \leqslant t \leqslant t_p(\lambda, \theta)$

$$P_t = H_b(\lambda, \theta) - \sin\theta \int_0^t f(s)\,\mathrm{d}s, \tag{8a}$$

$$P = H_b(\lambda, \theta)\, t - \sin\theta \int_0^t \int_0^{t'} f(s)\,\mathrm{d}s\,\mathrm{d}t', \tag{8b}$$

and at $t = t_p$

$$H_p = H_b(\lambda, \theta) - \sin\theta \int_0^{t_p(\lambda,\theta)} f(s)\,\mathrm{d}s. \tag{8c}$$

From $(8b)$ we can show that if the zonal velocity is positive at some depth it must be positive at lesser depths. The specified Sverdrup function requires that the zonal transport be positive at the western boundary from θ_n southwards to the latitude where $(\partial/\partial\theta)\, w_e \sin^2\theta = 0$. Hence the zonal velocity at the surface must be positive, fluid must emerge as unventilated from the sidewall, and $H_p = 0$ along the northern reaches of the western boundary in the range $\theta_w^* \leqslant \theta \leqslant \theta_n$ where $u(0, \theta_w^*, t_0) = 0$. With $f(t)$ given, equation (4) at $\lambda = 0$ yields,

$$\sin^2\theta \int_0^{t_0} \left(\int_t^{t_0} f(s)\,\mathrm{d}s \right)^2 \mathrm{d}t = S(0, \theta).$$

This expression can be utilized to determine $t_0(0, \theta)$ and

$$H_b(0, \theta) \left(= \sin\theta \left(\int_0^{t_0} f\,\mathrm{d}s \right) \right).$$

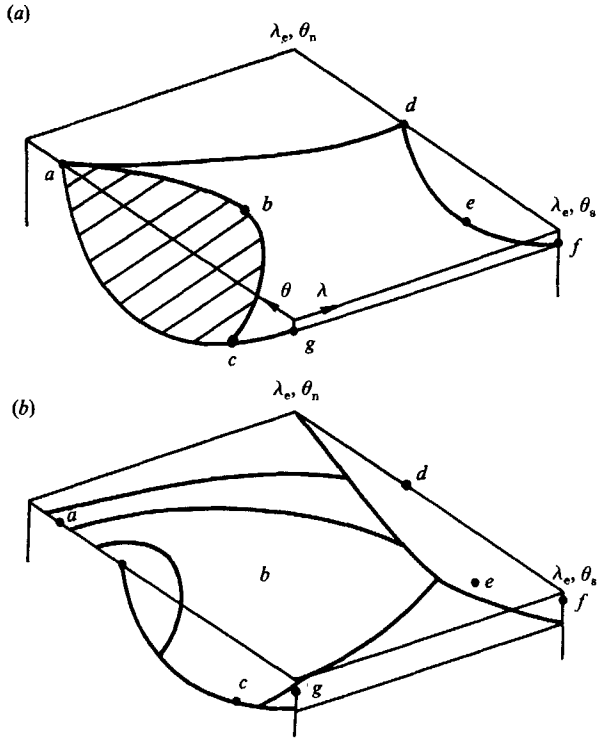

FIGURE 1. (*a*) Sketch of an outcropping isopycnal surface showing ventilated and unventilated (shaded) regions. (*b*) Sketch of the partitioning surfaces with points in (*a*) indicated.

The Bernoulli function for streamlines leaving the western wall at the surface with $\theta_w^* \leqslant \theta_w \equiv \theta < \theta_n$ is given by

$$P_w(t_0) = P(0, \theta, t_0) = \sin\theta_w(t_0)\left[t_0 \int_0^{t_0} f(s)\,ds - \int_0^{t_0}\int_0^{t} f(s)\,ds\,dt\right], \tag{9}$$

where $t_0 = t_0(0, \theta_w)$.

Now consider the material surface composed of the streamlines leaving the western boundary at the surface; the Bernoulli function is a constant along streamlines. This material surface is clearly part of the partitioning surface. Fluid above this surface cannot have originated on the western wall and must have downwelled from the free surface. We follow a parcel with density t_1 from the western wall at the surface as it moves southwards and downwards to an interior location λ, θ. Along this streamline $t_p = t_1$. Setting the *in situ* value of P, equation (8*b*), to $P_w(t_1)$ from (9) allows us to obtain, dropping subscripts on $t_p = t_1$,

$$H_b = \sin\theta_w(t)\int_0^t f(s)\,ds + (\sin\theta - \sin\theta_w(t))\int_0^t\int_0^{t'} f(s)\,ds\,dt'/t.$$

Also,

$$H_p = H_b - \sin\theta\int_0^t f(s)\,ds,$$

or

$$\frac{H_p}{H_b} = \frac{1-\sin\theta/\sin\theta_w(t)}{1+A(t)\sin\theta/\sin\theta_w(t)}, \tag{10a}$$

where
$$A = 1 - \int_0^t s(t-s)\frac{\mathrm{d}f}{\mathrm{d}s}\mathrm{d}s \Big/ \int_0^t sf(s)\,\mathrm{d}s. \tag{10b}$$

If f is a constant, $A = 1$. If $f = c_1/t^{\frac{1}{2}}$ then the magnitude of the density gradient vanishes at the thermocline base and increases upwards and $A = 2$. Equation (10) shows us that the partitioning depth is only a small fraction of the total depth. It is maximized when $\theta_w = \theta_n$ at any latitude θ. If a streamline penetrates southwards to a latitude of $\theta = 30°$, then $H_p/H_b < 0.22$ for $A = 1$ and $H_p/H_b < 0.16$ for $A = 2$. The smallness of this ratio in the subtropical regions, a result which is independent of the ventilated potential vorticity function, implies, as we see below, that the ventilated field has a negligible effect on H_b and hence H_p and t_p. The effect of the ventilated region on the partitioning fields is felt solely through the Sverdrup relation.

$$\int_0^{t_p} P_t^2\,\mathrm{d}t + \int_{t_p}^{t_0} P_t^2\,\mathrm{d}t = S(\lambda,\theta). \tag{11}$$

The first integral on the right-hand side is $O(H_b^2 t_p)$ while the second is $O(H_p^2(t_0 - t_p))$. In subtropical latitudes where $H_p/H_b \ll 1$, $t_0 - t_p \approx O(1)$ and $H_b \approx O(1)$, the second integral on the left-hand side of (11) is negligible ($O(H_p^2/H_b^2)$) relative to the first. Neglecting this integral, one may solve for H_b from (11) and so determine H_p and t_p.

We conclude that in subtropical regions, if $\mathrm{d}f/\mathrm{d}t \leqslant 0$, the normal case, the ventilated region is thin and the surface density fields has a negligible impact ($O(H_p/H_b)^2)$) on the thermocline depth, the partitioning fields, and the flow in the unventilated region ($-H_b \leqslant z \leqslant -H_p$). The velocity at the base of the ventilation region is $O(H_b t_p)$ and the changes in velocity from $z = -H_p$ to the surface is $O(|\nabla t_0| H_p)$. Hence the relative effect of the surface density field on surface velocities is $O(|\nabla t_0| H_p/H_b t_p)$; this is greater than the effect of surface density on H_b and H_p but is still small in subtropical regions. Hence the unventilated vorticity field and the Sverdrup function are the principal determinants of the motion in subtropical regions.

An inverse procedure can be used to determine the flow in these regions. At a given latitude, θ, we choose a value for H_b. We then find a value for t ($= t_p$) which sets the *in situ* value of P (equation (8*b*)) equal to $P_w(t)$ (equation (9)); with H_b, θ, and t_p now known, we find H_p from (8*c*). Neglecting the second integral on the right-hand side of (11), we use this equation to determine S and hence λ where the chosen value of H_b exists and so complete the solution in the recirculating region at θ, λ.

The results of J and the following section indicate that the material surface composed of fluid originating at $\lambda = 0$, $\theta_w^* \leqslant \theta \leqslant \theta_n$ covers all but the extreme southern and southeastern portions of the gyre. Streamlines originating at $\lambda = 0$, at $z = 0$, very near θ_n, end on the eastern boundary while streamlines originating further south on the western boundary also terminate there after looping clockwise through the interior. A streamline with density t_e^* and $P = P_w(t_e^*)$ leaving near the northern boundary will just graze the eastern boundary at θ_e^* before returning to the western boundary, see figure 2. The southern leg of this grazing streamline forms the southern boundary of the portion of the partitioning surface formed by streamlines of western boundary origin. The remainder of the partitioning surface is composed of streamlines of eastern-boundary origin issuing forth for $\theta \leqslant \theta_e^*$ at the depth where the zonal velocity vanishes.

The results in J as well as the next section show that while the zonal transport vanishes at the eastern boundary, deep waters emerge from this boundary ($u < 0$) while fluid nearer the surface flows into the boundary, see figure 3. We consider a

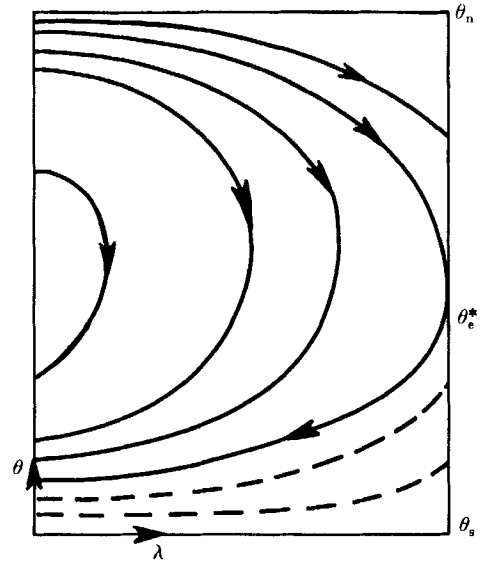

FIGURE 2. Sketch of streamlines in the partitioning surface. Solid lines are of western origin while dashed lines are of eastern origin.

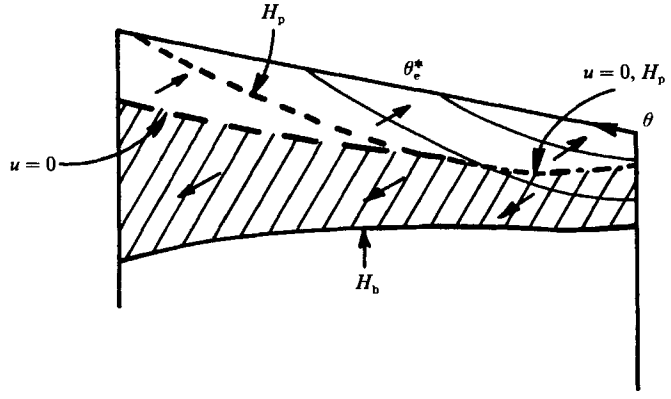

FIGURE 3. Sketch of zonal velocity at eastern boundary as viewed from the west. The shaded area is outflowing and solid lines are intersections of isopycnal surfaces with the eastern boundary.

streamline originating at $\lambda = \lambda_e$ south of θ_e^* at the point $u = 0$. Fluid below this point is unventilated and is flowing westward in the gyre while the fluid above this streamline is of surface origin as it cannot have originated on the western boundary nor at the eastern wall further to the north, as this is an inflow region for these isopycnals.

Thus the partitioning surface is composed of streamlines of surface-western-boundary origin north of the southern leg of the grazing streamline and of eastern-boundary origin south of this leg. We note that only if t_0 is specified to be less than the computed value of t_p, for a given $f(t)$, does this procedure break down. In the next section we perform a simple calculation which demonstrates the procedure outlined above and verifies our conclusions about the small impact of the surface density field on the flow in subtropical regions.

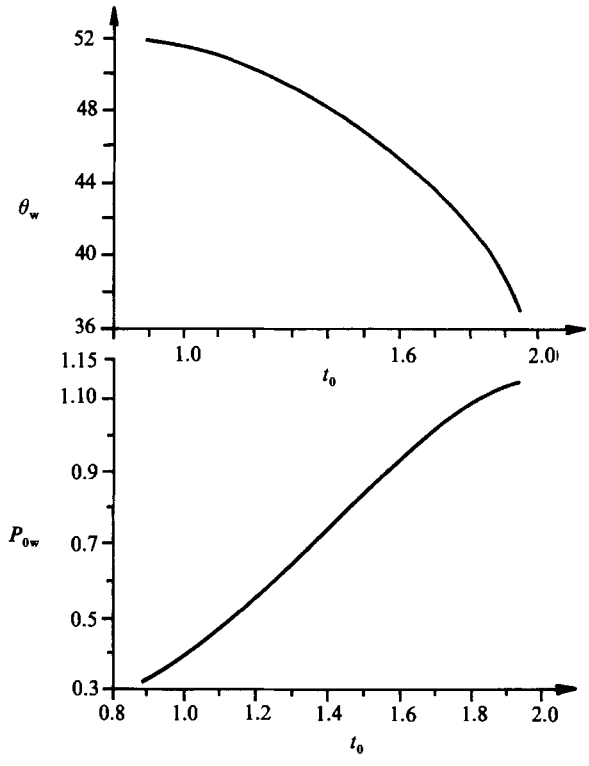

FIGURE 4. The surface pressure, P_{0w} and latitude at the western boundary ($\lambda = 0$), as functions of surface density t_0.

4. An example of partitioned model

To demonstrate the insensitivity of partitioning fields to the surface density fields in subtropical regions, we choose the unventilated potential vorticity function, $f(t)$, to be equal to 1.0 and the ventilated function to be a constant, γ (< 1). We note that the conventional ventilated vorticity equals $1/\gamma$ (> 1). The potential vorticity equation ($3a$) can be integrated subject to ($3b$), ($3d$), and the continuity of P and P_t across t_p to yield the following results:

for $0 \leqslant t \leqslant t_p$,

$$P = H_b(\lambda, \theta)\, t - \tfrac{1}{2}\sin\theta t^2, \tag{12a}$$

$$H_p = H_b - \sin\theta t_p, \tag{12b}$$

$$P_p = P(\lambda, \theta, t_p) = t_p(H_b - \tfrac{1}{2}\sin\theta t_p); \tag{12c}$$

for $t_p \leqslant t \leqslant t_0$,

$$P = P_p + H_p(t - t_p) - \tfrac{1}{2}\gamma \sin\theta (t - t_p)^2, \tag{12d}$$

$$t_0 = t_p + H_p/\gamma \sin\theta, \tag{12e}$$

$$P_0 = P(\lambda, \theta, t_0) = P_p + H_p^2/2\gamma \sin\theta. \tag{12f}$$

The Sverdrup condition requires

$$S(\lambda, \theta) = (H_b^3 - H_p^3)/3\sin\theta + H_p^3/3\gamma\sin\theta, \tag{13a}$$

or

$$H_b^3 + ((1-\gamma)/\gamma)\, H_p^3 = 3S(\lambda, \theta)\sin\theta. \tag{13b}$$

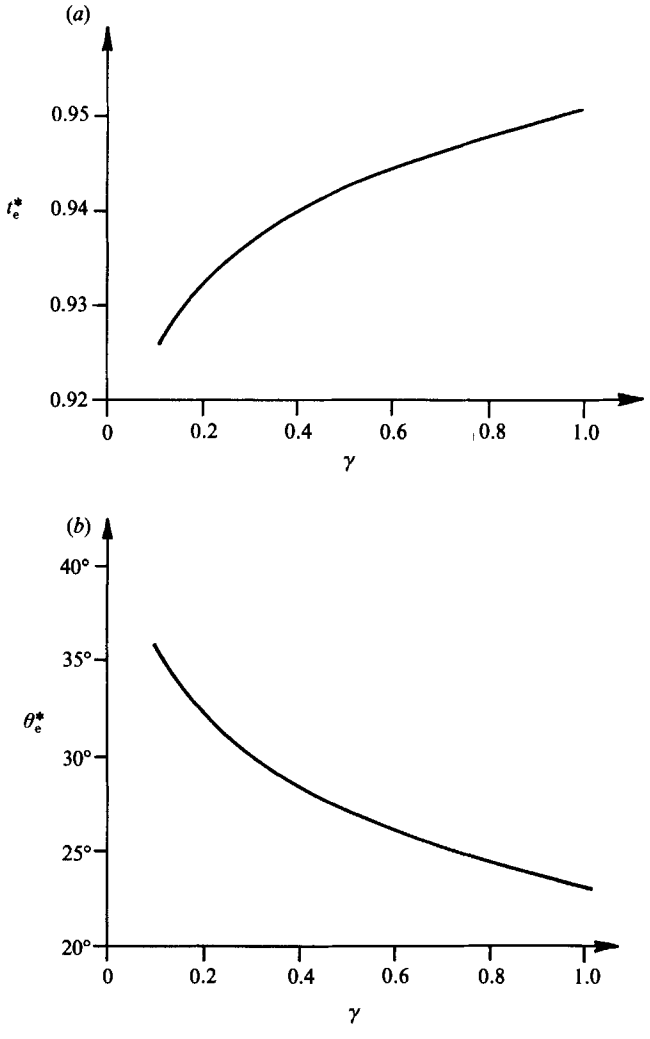

FIGURE 5. Grazing streamline characteristics as a function of γ. (*a*) The density of the grazing streamline. (*b*) The latitude of the grazing streamline at $\lambda = \lambda_e$.

In figure 4, we present $P_w(t)$ and $\theta_w(t)$ as functions of t; these results follow from equations (7*a*, *b*) with $\lambda = 0$. As indicated earlier north of the southern leg of the t_e^* streamline we choose a value for $\sin\theta$ and H_b and determine t_p by setting the *in situ* value for P, equation (12*a*), equal to P_w. In practice we find t_p by increasing t above t_{0n} until the two Bernoulli functions are equal. We then use (12*b*) to find H_p. As the left-hand side of (13*b*) is known exactly we solve this equation for $S(\lambda, \theta)$ and hence λ. The Sverdrup equation can thus be solved exactly. At each latitude eleven values of H_b are specified and λ computed for each depth. To find the thermocline depth at a prescribed λ, we linearly interpolate using values of H_b at bracketing longitudes previously calculated. The value of λ at this interpolated value of H_b is then computed and is generally within 0.0001 of the prescribed value.

We must now determine the grazing streamline characteristics and the partitioning surface south of the southern leg of this streamline. For a partitioning streamline

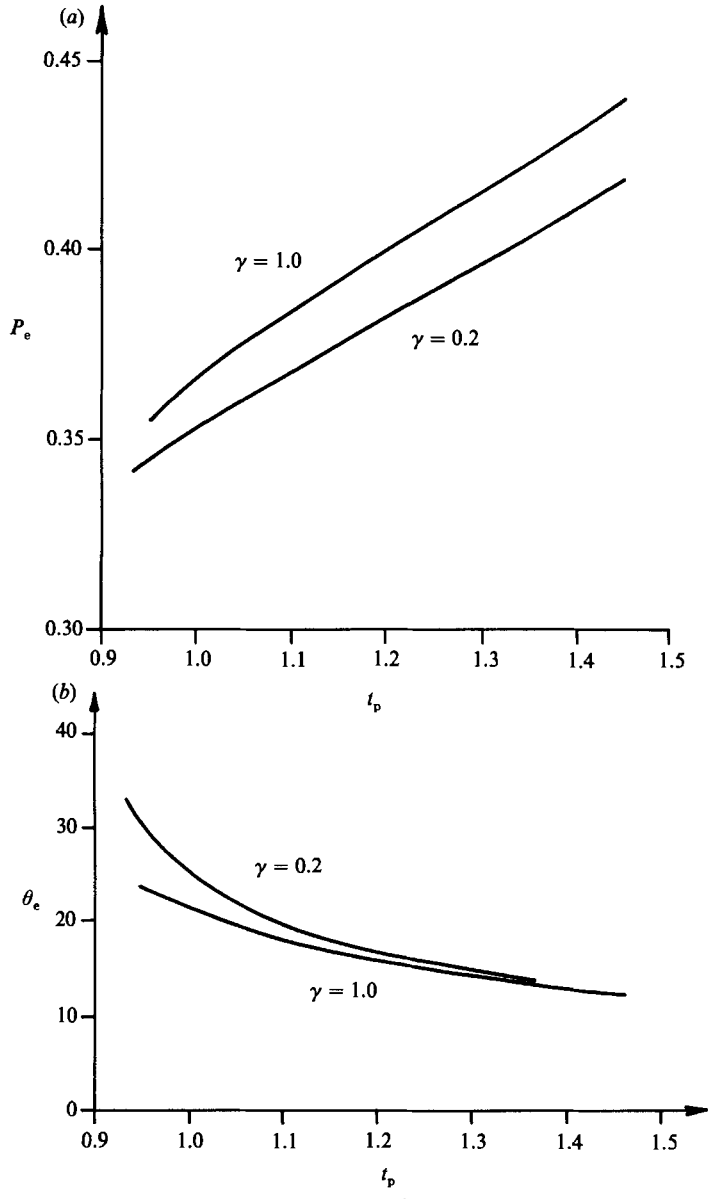

FIGURE 6. Characteristics of the partitioning surface south of the grazing streamline. (*a*) $P_e(t_p)$, (*b*) $\theta_e(t_p)$ for $\gamma = 0.2$.

originating on the western boundary $P_w(t) = \frac{1}{2}\sin\theta_w(t)\,t^2$, with the p subscripts dropped. From (12*b*, *c*) along this streamline

$$H_b = \tfrac{1}{2}(\sin\theta_w + \sin\theta)\,t, \tag{14a}$$

$$H_p = \tfrac{1}{2}(\sin\theta_w - \sin\theta)\,t. \tag{14b}$$

Using this expression in (13*b*), the Sverdrup condition leads to

$$((1+r)^3 + ((1-\gamma)/\gamma)\,(1-r)^3)\,(t\sin\theta_w(t))^3 = 24S(\lambda,\theta)\sin\theta, \tag{15a}$$

where

$$r = \sin\theta/\sin\theta_w(t). \tag{15b}$$

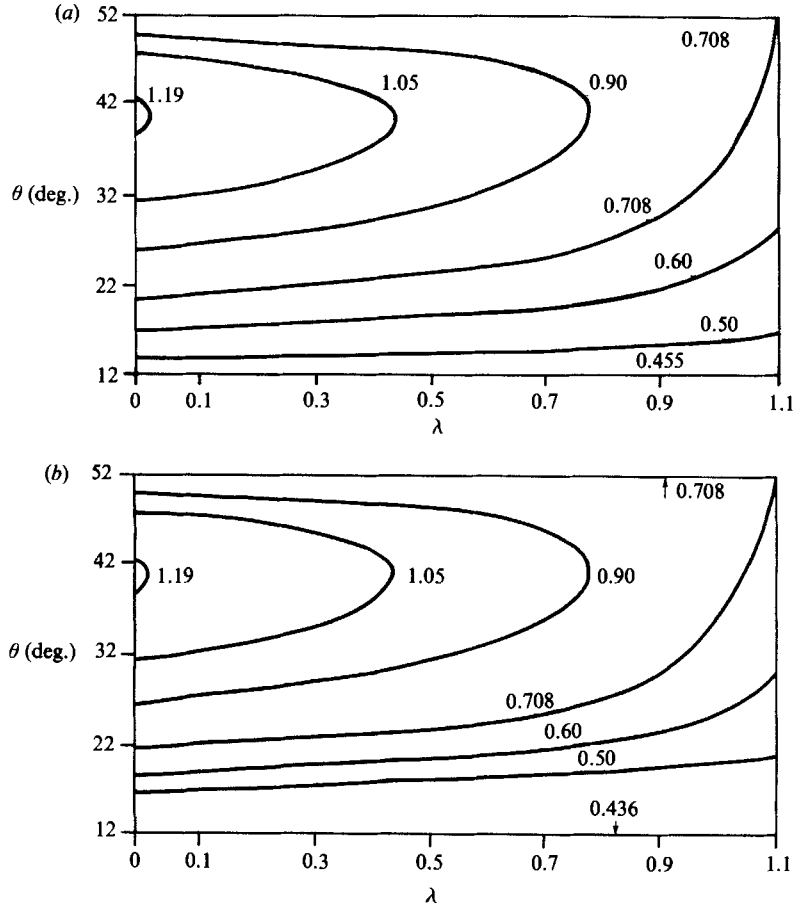

FIGURE 7. The non-dimensional thermocline depth, H_b. (*a*) $\gamma = 1.0$, (*b*) $\gamma = 0.2$.

With t fixed, (15) is the trajectory of a partitioning streamline of western boundary origin which may be solved for λ as a function of θ and t. For the grazing streamline, at $\lambda = \lambda_e$, $\theta = \theta_e^*$, $S = C$ and $d\lambda/d\theta = 0$. These two conditions allow us to solve for t_e^* and θ_e^* as function of γ. These results are shown in figure 5. As γ decreases from 1.0, t_e^* decreases slightly and θ_e^* increases. For any value of γ we can determine H_b at λ_e and θ_e^* using (14*a*) evaluated at θ_e^*.

The partitioning surface south of the grazing streamline consists of the material surface composed of streamlines originating at λ_e south of θ_e^* at the value of $t = t_p$ where $u = 0$. Hence at λ_e, for $\theta < \theta_e^*$, from (12*a*) we find $t_p = 2H_{b\theta}/\cos\theta$. Hence at λ_e

$$H_p = H_b - \sin\theta t_p = H_b - 2H_{b\theta}\sin\theta/\cos\theta. \tag{16}$$

Substituting this expression into (13*b*) at $\lambda_e (S = C)$ yields a first-order ordinary differential equation for $H_b(\theta)$ at λ_e south of θ_e^* with $H_b(\theta_e^*)$ known. This equation can be integrated numerically from θ_e^* southwards to θ_s to determine H_b then t_p and $P_e(t_p)$. We note that for $\gamma = 1$, $H_b = (3C\sin\theta)^{\frac{1}{3}}$ and $t_p = 2H_b/3\sin\theta$. In figure 6 we present the results for $\gamma = 1.0$ and $\gamma = 0.2$ for $C = 0.15$.

The partitioning fields in the interior south of the grazing streamline are determined by choosing eleven values of H_b at a fixed θ and then finding the value of $t = t_p$ which sets the *in situ* value of P (12*a*) equal to $P_e(t)$. With t_p and hence H_p

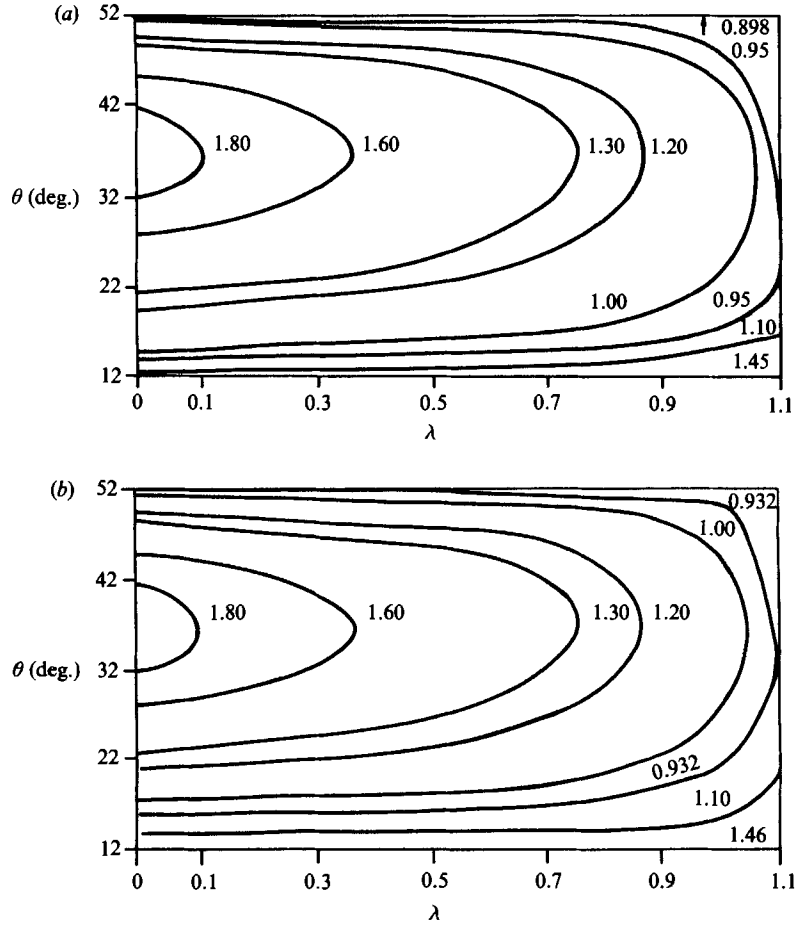

FIGURE 8. The partitioning density field, t_p. (*a*) $\gamma = 1.0$, (*b*) $\gamma = 0.2$.

determined the Sverdrup relation is used to determine λ for the selected value of H_b and θ. Interpolation is then used to find the partitioning fields at specific values of λ.

5. Numerical results

We now specify parameter values. We take $W = 10^{-6}$ m/s, $r = 6370$ km, $g = 9.8$ m/s^2, $2\Omega = 1.45 \times 10^{-4}$/s, $\Delta\rho/\rho_1 = 0.56 \times 10^{-3}$ and $C = 0.15$. We find $D = 1040$ m and $t_{0n} = 0.898$.

We present calculations for $\gamma = 1.0$ and 0.2. In figures 7, 8 and 9 we present the thermocline depths for both values of γ, the partitioning density for both cases, and the partitioning depths for both cases. For both values of γ, H_p is small north of $\theta = 25°$ and decreases with latitude. The ventilated fluid is thus confined to a relatively thin layer north of this latitude. Further the difference in H_b, H_p, and t_p for $\gamma = 1.0$ and $\gamma = 0.2$ is at most 3% at $\theta = 25°$, at most 1.5% at $\theta = 30°$ and considerably smaller further to the north. The insensitivity of the partitioning fields and H_b to the ventilated vorticity north of $\theta = 25°$ is consistent with our basic conclusions. As we have shown, in this region $t_p = t_p(H_b, \theta)$ and $H_p = H_p(H_b, \theta)$. The ventilated vorticity

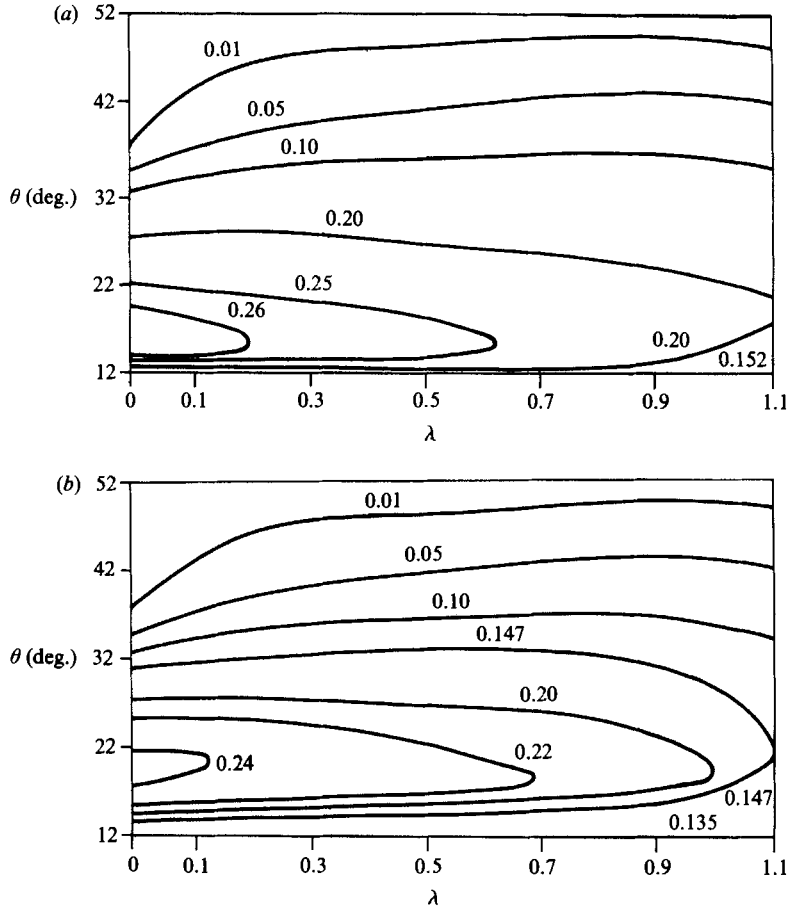

FIGURE 9. The non-dimensional partitioning depth field, H_p. (*a*) $\gamma = 1.0$, (*b*) $\gamma = 0.2$.

does not affect these two functions. Only when we satisfy the Sverdrup condition does γ appear. In (13*b*) we note that the relative effect of γ is $(1-\gamma)H_p^3/\gamma H_b^3$. Since H_p/H_b decreases rapidly as θ increases the effect of γ decreases even more dramatically.

We next turn to the surface density and surface Bernoulli fields presented in figures 10 and 11 respectively. The difference in t_0 for the $\gamma = 1.0$ and $\gamma = 0.2$ case is significant and follows from (12*e*), *viz.* $t_0 = H_p/\gamma \sin\theta + t_p$. If H_p and t_p are nearly the same for the two cases, then Δt_0, the change in t_0 between the two, is $4H_p/\sin\theta$. At $\theta = 30°$ with $H_p \sim 0.15$, $\Delta t_0 = 1.2$. The surface pressure fields show some variation with γ and $\Delta P_0 = \frac{1}{2}H_p\,\Delta t_0$ or about 8% of the change in t_0.

We next turn to gyre structure and flow. In figures 12 to 15 we show the depths and pressure fields for the $\gamma = 0.2$ case for $t = 0.5$, 1.0, 1.5 and 2.5. The unventilated regions are shown shaded. The depth of the $t = 0$ surface is of course H_b. For $t = \epsilon \ll 1$, $P = H_b\epsilon + O(\epsilon^2)$ so the H_b contours (figure 7*b*) are streamlines for small values of t. The results for $H(\lambda, \theta, t)$ and $P(\lambda, \theta, t)$ are in general quite similar to those in J. The ventilated surfaces whose outcrop lines intersect $\lambda = 0$ north of 37°, i.e. the $t = 1.0$ and 1.5 surfaces, have unventilated regions shades. The $P = 0.822$ streamline in the $t = 1.5$ surface separates ventilated and unventilated regions. The location of the ventilated region is consistent with data given in Rhines (1986) for a partially

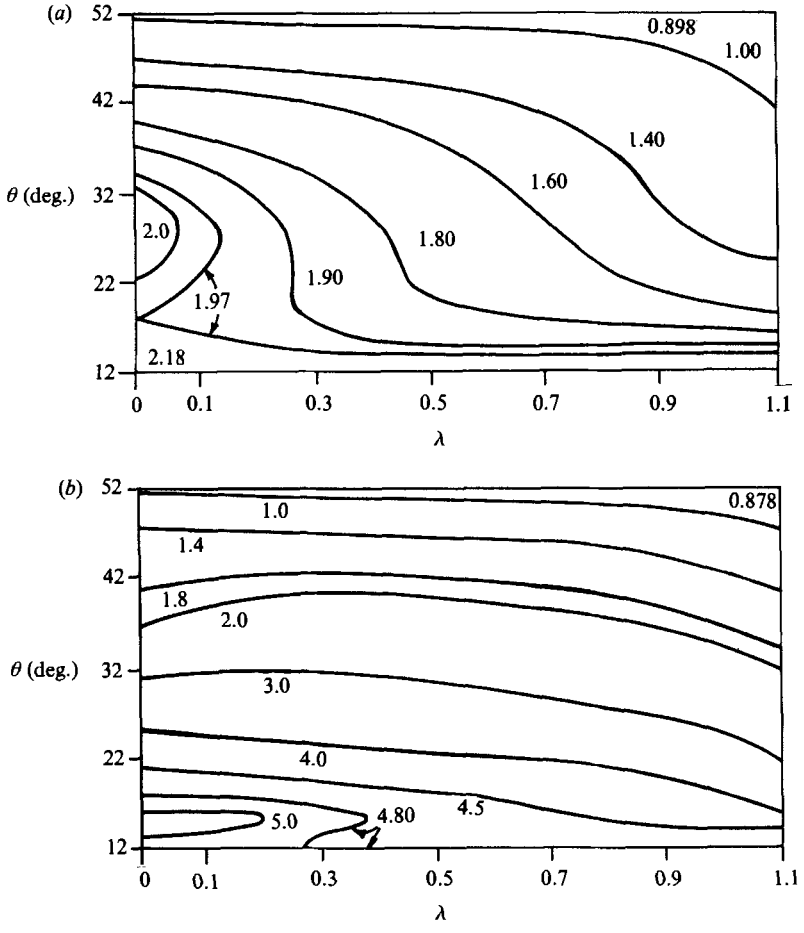

FIGURE 10. Contours of constant t_0, the negative of the surface density anomaly. (*a*) $\gamma = 1.0$, (*b*) $\gamma = 0.2$.

ventilated surface. Ventilated waters occupy the shallowest regions of this isopycnal surface. Ventilated fluid fills much of this shallow surface. The $t = 2.5$ surface is entirely filled with ventilated fluid most of which flows from the outcrop line into the western boundary.

As we have seen, the partitioning fields are relatively insensitive to the ventilated potential vorticity in subtropical regions.

6. Comparison with earlier work

In this section, we compare our model predictions with those of several other works. We briefly review those of our predictions which will be used for comparisons. Our model predicts clockwise motion in all layers above the stagnant homogeneous layer; flow occurs in totally or partially ventilated surfaces as well as in those surfaces which are totally unventilated. The thermocline base, with the use of parameters specified in the previous section, ranges from a depth of 1200 m at the eastern wall at 40 °N to a depth of 460 m at the southern boundary of the gyre. At the eastern boundary where the zonal transport is taken to vanish, there is weak

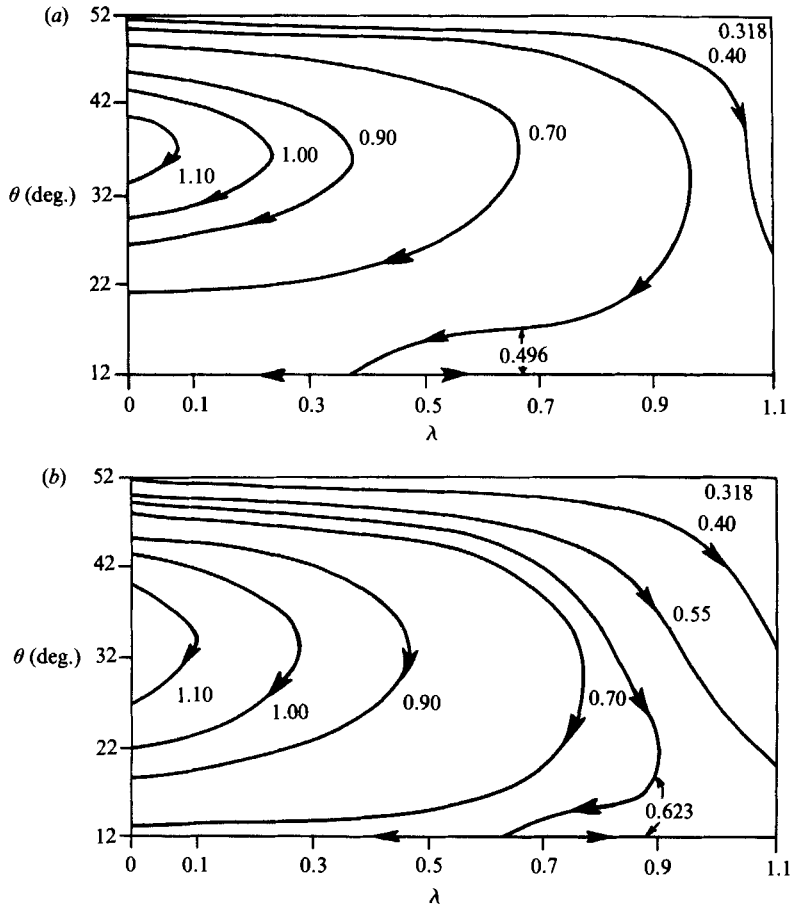

FIGURE 11. The surface pressure field, P_0. (*a*) $\gamma = 1.0$, (*b*) $\gamma = 0.2$.

outflow at depth and inflow nearer the surface. The maximum outflow speed is 0.77 cm/s at θ_s and the mean outflow speed ($0.53C^{\frac{2}{3}}$) is 0.09 cm/s. The total outflow from this boundary at depths below ($-\frac{1}{3}H_b(\theta)$) is 1.6 Sverdrups ($0.26C$). The maximum change in Bernoulli functions as we move along the eastern boundary down an isopycnal surface which outcrops at θ_0 to the point of maximum P is only 1.5 mb ($0.43\,(9C^2/\sin\theta_0)^{\frac{1}{3}}$) for surfaces outcropping near the northern boundary. The overall change in P from the outcrop point at θ_0 to θ_s is 0.35 mb. This small change reflects the weak zonal velocities at $\lambda = \lambda_e$. The east to west variation of P in these surfaces which outcrop near θ_n is typically 30 mb. At the western boundary our theory predicts outflow at all depths ($-H_b \leqslant z \leqslant 0$) to the north, inflow at all depths to the south and a transitional region with inflow at depth and outflow nearer the surface. We first compare our results to Cox & Bryan (1984; hereinafter referred to as CB). Theirs is a time-dependent finite-difference numerical model which is run to steady state. The model includes nonlinear terms in the horizontal momentum equations, and horizontal and vertical turbulent mixing terms in both the horizontal momentum equations and the density equation; the turbulent effects are modelled using constant eddy diffusivities. The model is driven by wind-stress and buoyancy-flux conditions applied at the surface (for their $\tau_0 = 1$ case). The domain extends from an eastern to a western wall and includes gyres to the north and south of the subtropical

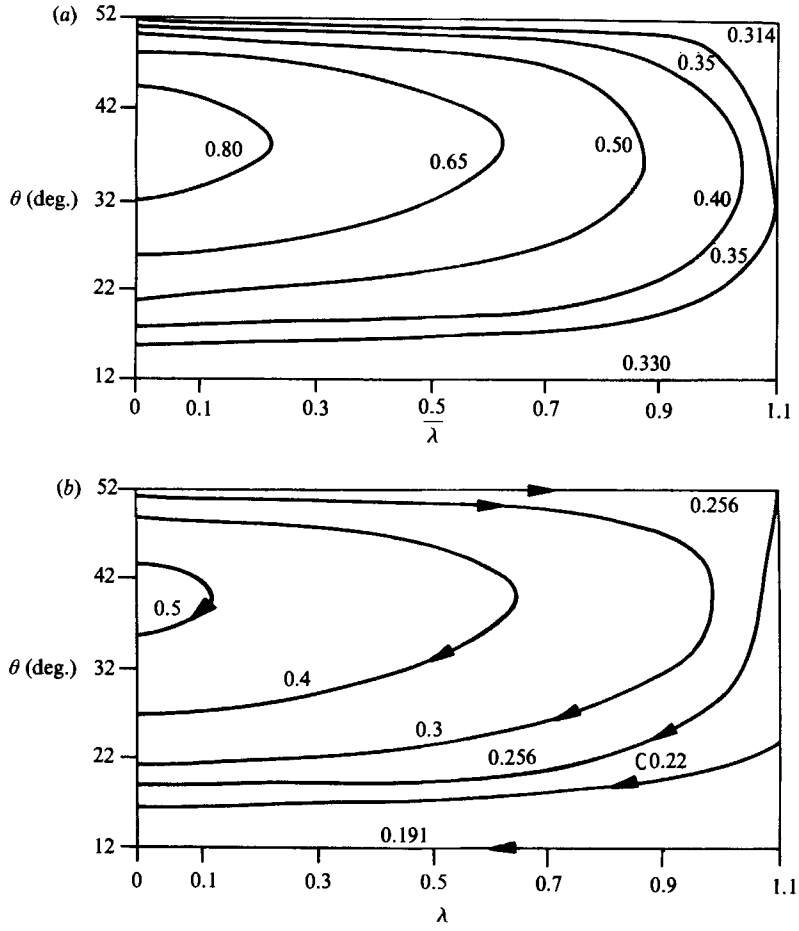

FIGURE 12. (*a*) The dimensionless depth, H, and (*b*) the Bernoulli function, P, for $\gamma = 0.2$ in the surface $t = 0.5$.

gyre; our comparisons are limited to the subtropical gyre. Further their calculations include both the dissipative upper mixed layer as well as the dissipative sidewall regions. As our calculations exclude these regions, comparisons are generally made outside the mixed and sidewall regions. We note that small changes in density do occur in their model predictions outside these boundary layers but the major changes in density occur in the dissipative regions. Our comparisons will be made for their $\tau_0 = 1$ case wherein the motion is both wind and buoyancy driven.

Figure 2 of CB for $z = 0$ shows the surface pressure field. This is in good qualitative agreement in the subtropical gyre portion of their results with our figure 11 and shows inflow at the surface at the eastern boundary. Figure 5 of CB shows the velocity field in the eastern zone as a function of latitude. This figure shows weak zonal outflow at depth and inflow nearer the surface with the zero zonal flow curve increasing in depth to the north; again this is in agreement with our model predictions. Figure 4 of CB shows the velocity at mid-longitude. Parcel speeds are finite above, say, 750 m; in particular, Flows are finite near the 500 m depth and in the southern zone in a layer of fluid that does not outcrop in the subtropical gyre, i.e. in an unventilated region. This is consistent with our predictions of clockwise flow in

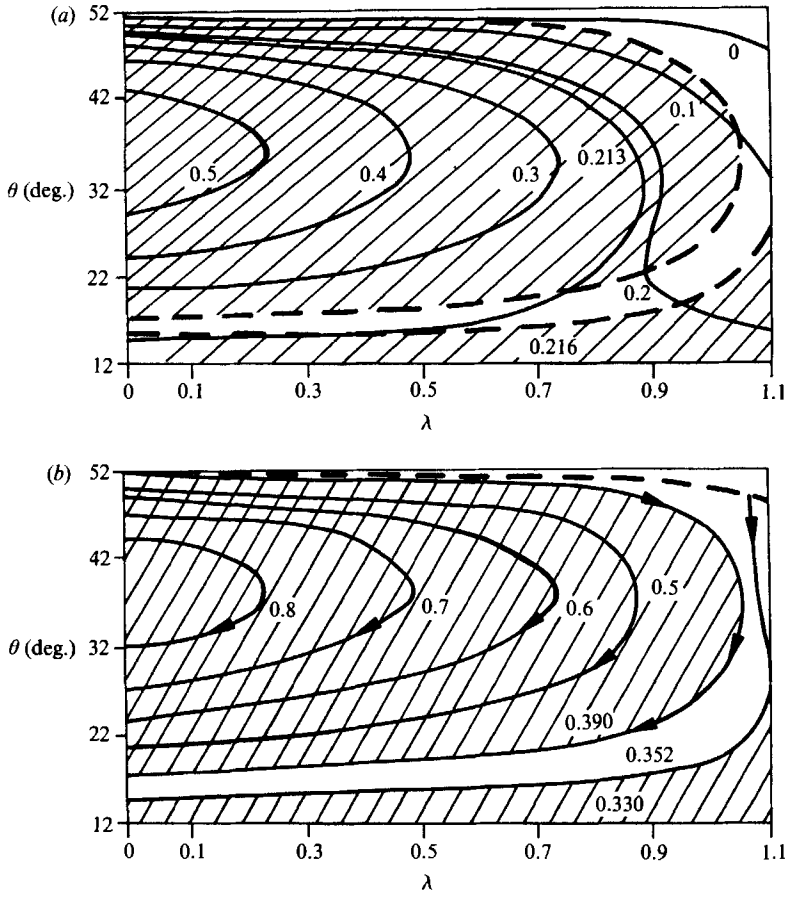

FIGURE 13. (*a*) The dimensionless depth, H, and (*b*) the Bernoulli function, P, for $\gamma = 0.2$ in the surface $t = 1.0$.

all isopycnal surfaces, ventilated or not. Figures 9(*b*, *c*, *d*) of CB show streamline patterns in three isopycnal surfaces which outcrop near the northern gyre boundary which is about 48 °N in their model. Clockwise flow is evident in all gyres. Overall changes in P in these surfaces range from 25 to 30 mb. The shrinking of the recirculating region is evident as surfaces outcrop further to the south. No inflow or outflow is evident on the eastern boundary, but the contour interval of 4 mb is too large to show the small variations in P predicted by our model at $\lambda = \lambda_e$.

We next turn to comparison with layered models. The model of Pedlosky & Young (1983) is chosen for comparison purposes as it is more general than that of Rhines & Young (1981) in allowing finite variations in the depth of isopycnal surfaces. Pedlosky & Young also include a deep unventilated layer as well as a latitudinal variation in the surface density field. Layered models typically require that the zonal speed vanish in each layer at the eastern boundary; in our work only the net zonal transport is required to vanish. The vanishing of the zonal velocity in each layer at $\lambda = \lambda_e$ in the work of Pedlosky & Young has, as an immediate consequence, the confinement of flow in unventilated layers to the northwest quadrant of the gyre. This is in direct contrast with our result that flow exists everywhere in the unventilated region. The evidence as to the proper eastern-boundary conditions from

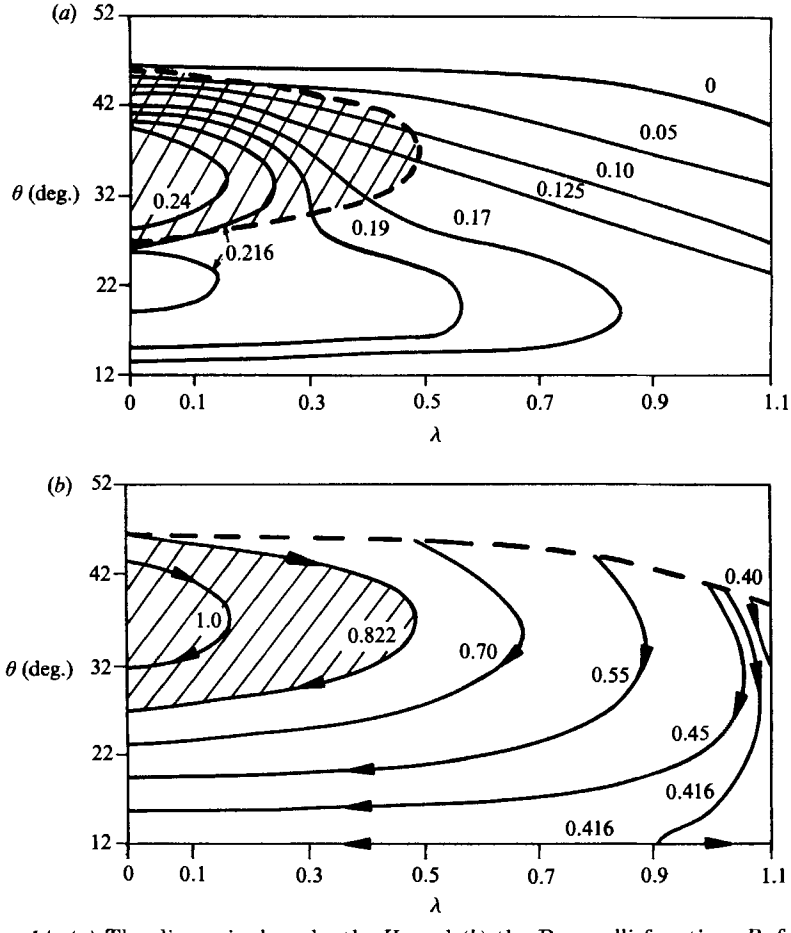

FIGURE 14. (*a*) The dimensionless depth, H, and (*b*) the Bernoulli function, P, for $\gamma = 0.2$ in the surface $t = 1.5$.

the BC numerical model is mixed. While figures 2 and 5 of CB indicate that there is inflow and outflow at the eastern boundary consistent with our results, figure 9 (*b*, *c*, *d*) leads to an uncertain result because of the relatively large contour interval taken for the Bernoulli function. However figure 4 of CB which shows flow in unventilated regions far from the northern gyre boundary is consistent with our results but in direct contrast to the stagnant flow prediction of Pedlosky & Young (1983).

The results of the present work are consistent with the those of Cox & Bryan (1984) though they contrast sharply with the results of Pedlosky & Young (1983); the contrast is traced to the eastern-boundary condition, a condition which is unclear at the present time.

We next turn to two recent continuously stratified models. The model of Killworth (1987) utilizes the density as an independent variable and extends the model developed in J to an infinite depth ocean. More relevant to the present work is the section in that paper wherein an unventilated layer with $\pi = f(t)$ is introduced above the stagnant homogeneous layer and below an active region where $\pi = G(t)P$. The potential vorticity equation is then integrated downward through the active region from the surface where a surface-density and Ekman-section condition is applied. The potential vorticity equation is integrated upwards through the unventilated

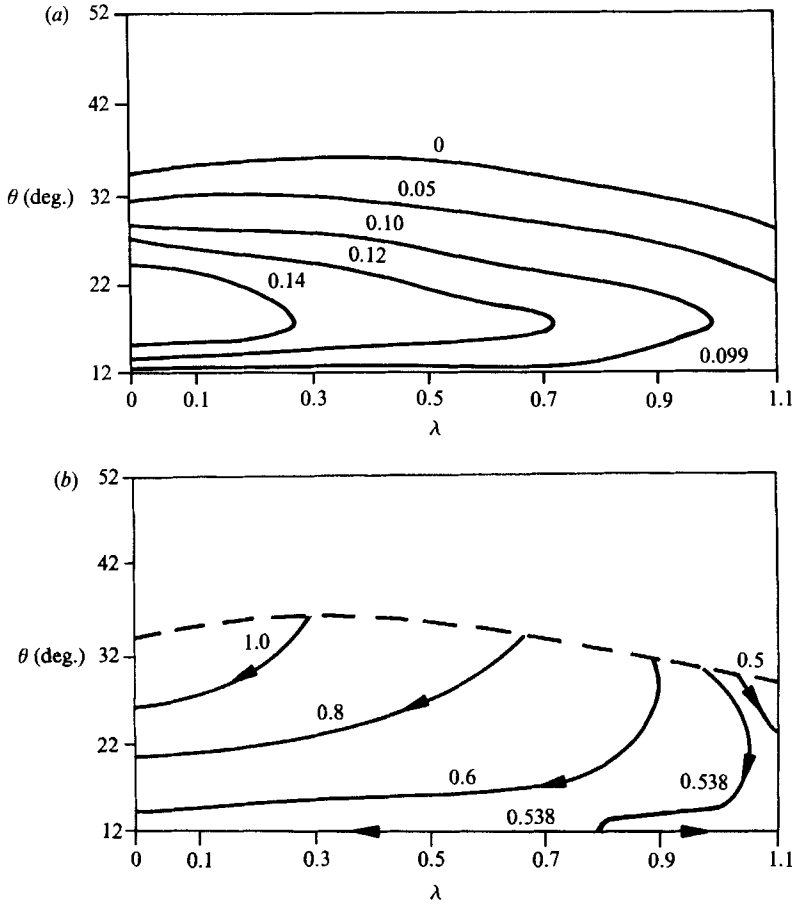

FIGURE 15. (*a*) The dimensionless depth, H, and (*b*) the Bernoulli function, P, for $\gamma = 0.2$ in the surface $t = 2.5$.

region to that density t_b where both P and P_t as given from both integrations match. However, the t_b field of Killworth is not the same as t_p given here, as fluid immediately above t_b may originate either at the surface or the sidewall. Isopycnal surfaces that outcrop and intersect the western boundary in the northern regions where the surface zonal flow is outwards must contain regions of fluid of western-boundary origin; in the present work we take $\pi = f(t)$ in the unventilated portion of outcropping isopycnal surfaces as well as in deeper totally unventilated surfaces. In Killworth this partitioning in an isopycnal surface is not imposed. As t_b from Killworth and t_p from the present work do not have the same meaning we attempt no comparisons.

A second recent continuously stratified model to be considered is that of Huang (1986). He utilizes z as the independent variable and three data derived forms of π; the form of π utilized depends strictly on the density and is not partitioned with respect to P as in the present work. The potential vorticity equation is integrated downwards from the base of the mixed layer at which point a surface-density and an Ekman-suction-derived condition are specified; no lower boundary condition is or can be imposed. The solution is assumed to be valid for all z at values of λ and θ where the vertical velocity becomes small at great depths and is assumed valid in the upper

portion of the water column if the vertical velocity does not tend to zero at great depths. This ignores the possibility that a lower boundary condition imposed at a specific value of z or density may affect the flow throughout the water column. As the focus is not on partitioning of the flow, no comparison with this work is undertaken.

7. Conclusions

As we have shown in the general case and verified in a calculation, the flow in most of the subtropical gyre is insensitive to the surface density field away from the surface outflow region of the western boundary. The principal determinants of the motion are the Sverdrup function and the unventilated potential vorticity function.

REFERENCES

Cox, M. B. & Bryan, K. 1984 A numerical model of the ventilated thermocline. *J. Phys. Oceanogr.* **14**, 674–687.

Huang, R. A. 1986 Solutions of the ideal fluid thermocline with continuous stratification. *J. Phys. Oceanogr.* **16**, 39–59.

Janowitz, G. S. 1986 A surface density and wind-driven model of the thermocline. *J. Geophys. Res.* **91**, 5111–5118.

Killworth, P. D. 1987 A continuously stratified non-linear ventilated thermocline. *J. Phys. Oceanogr.* **17**, 1925–1943.

Luyten, J. R., Pedlosky, J. & Stommel, H. 1983 The ventilated thermocline. *J. Phys. Oceanogr.* **13**, 292–309.

Pedlosky, J. 1983 Eastern boundary ventilation and the structure of the thermocline. *J. Phys. Oceanogr.* **13**, 2038–2044.

Pedlosky, J. & Young, W. R. 1983 Ventilation, potential vorticity homogenization, and the structure of ocean circulation. *J. Phys. Oceanogr.* **13**, 2020–2037.

Rhines, P. B. 1986 Vorticity dynamics of the oceanic general circulation. *Ann. Rev. Fluid Mech.* **18**, 433–497.

Rhines, P. B. & Young, W. R. 1981 Theory of the wind-driven circulation, I: Mid-ocean gyres. *J. Mar. Res.* **40**, suppl. 559–596.